View Online

A TIMS-based method for the high precision measurements of the three-isotope potassium composition of small samples

Daniel Wielandt* and Martin Bizzarro

Received 7th July 2010, Accepted 22nd October 2010
DOI: 10.1039/c0ja00067a

A novel thermal ionization mass spectrometry (TIMS) method for the three-isotope analysis of K has been developed, and ion chromatographic methods for the separation of K have been adapted for the processing of small samples. The precise measurement of K-isotopes is challenged by the presence of large isotope ratios in common K, and the accuracy of such measurements is compromised by isobaric interference and abundance sensitivity related issues. The combined expanded dynamic range and improved signal/noise ratio of a Triton TIMS with an adapted amplifier setup however allows measurements in the theoretically poisson-noise dominated intensity regime, while the high sensitivity of the thermal ionization-based source towards K allows this intensity regime to be reached, even with small samples. Analyses of 150 ng K samples of terrestrial basalts shows 2 s.d. 100 ppm-level or better reproducibility for mass fractionation corrected $^{41}K/^{39}K$ ratios, while 10 ng K samples show 2 s.d. 200 ppm-level or better for mass fractionation corrected $^{41}K/^{39}K$ ratios. The described methods are suitable for the high precision determination of internally mass fractionation corrected isotope anomalies in small samples, such as those recoverable from refractory inclusions in chondritic meteorites, or other low-level, rare or valuable materials. For meteoritic inclusions in particular, this has applications in the determination of ^{41}K excesses, attributable to the former presence of ^{41}Ca, and the reproducibility-levels reached are sufficient to resolve bulk radiogenic anomalies at the level suggested by prior ion microprobe studies. In addition to such radiometric applications, the K-isotope composition is potentially sensitive to cosmic ray overprint, and as such may be used to assess the level of cosmic ray irradiation in various extra-terrestrial materials.

Published on 11 November 2010 on http://pubs.rsc.org | doi:10.1039/C0JA00067A
Downloaded by New Copenhagen University on 26 February 2011

1 Introduction

High precision three-isotope measurements of K have interesting potential applications in the field of cosmochemistry, where they may resolve mass-independent ^{41}K anomalies in meteoritic materials, attributable to the former presence or isolation from decay of the shortlived ^{41}Ca radionuclide ($t_{1/2} \sim 100$ Kyr) in the early solar system. Such measurements may form the basis for tracing and dating based on this shortlived decay system. Because of the very short halflife of ^{41}Ca, the level of ^{41}Ca in the early solar system is highly sensitive to the timing of its nucleosynthesis relative to the formation of the solar system; therefore, it may help date and constrain the location and process of nucleosynthesis. For the same reasons, viable bulk based ^{41}Ca–^{41}K chronometry may reach high chronometric precisions.

The study of the ^{41}Ca–^{41}K-system has until now been carried out by secondary ion mass spectrometry (SIMS) analyses of refractory inclusions,[1] where microscopic domains with very high Ca/K-ratios of 10^5 to 10^8 contain ^{41}K excesses as large as ~1000%. The excesses are correlated with Ca/K ratios, consistent with the presence of ^{41}Ca at the level of $^{41}Ca/^{40}Ca \sim 1.4 \times 10^{-8}$. The suggested presence or absence of ^{41}Ca in refractory inclusions at the microscopic scale is coincident with the presence or absence of ^{26}Mg excesses, attributable to the former presence of ^{26}Al, suggesting a possible link between the source of the two shortlived radionuclides. This source has generally been interpreted as being stellar nucleosynthetic in nature,[2,3] and the suggested levels of both radionuclides have been utilized as boundary conditions in combined nucleosynthesis, mass transfer and free decay models for the stellar production and incorporation/injection of shortlived radionuclei into the nascent solar system.[4,5] In these models, the ^{41}Ca-level suggested by SIMS provides strict free decay time-constraints. Energetic particle irradiation has also recieved considerable attention as a possible source of some of the shortlived radionuclei, including ^{41}Ca (ref. 6 + 7).

The use of SIMS is however limited by the isotopic and isobaric peculiarities of K and Ca, *i.e.* the low abundance of ^{40}K, and the inability to resolve the ^{40}Ca–^{40}K isobaric interference at any available mass resolutions. SIMS-based studies therefore treat K as a *de facto* two isotope system, considering only the offline mass fractionation corrected $^{41}K/^{39}K$ ratio. This has made it necessary to disregard phases with low Ca/K ratios, and hence low expected ^{41}K excesses, since it would not be possible to distinguish and separate the expected small radiogenic excesses generated in low Ca/K-phases, from the inherent instrumental and natural stable isotope fractionation, uncorrectable by a two isotope method.

Another important limitation is that such two-isotope measurements cannot clearly distinguish between *in situ* decay of ^{41}Ca incorporated at formation, and overprint from the production of mass 41 nuclei production (ultimately ^{41}K) by

Centre for Star and Planet Formation, Natural History Museum of Denmark, University of Copenhagen, DK-1350 Copenhagen, Denmark. E-mail: wielandt@snm.ku.dh

 This journal is © The Royal Society of Chemistry 2011

View Online

Published on 11 November 2010 on http://pubs.rsc.org | doi:10.1039/C0JA00067A
Downloaded by New Copenhagen University on 26 February 2011

in situ cosmic ray spallation/neutron capture on stable Ca-isotopes. The relative spallogenic overproduction of ^{41}K compared to ^{39}K probably holds true in most matrices, including refractory inclusions, where the near-monopoly of Ca as a target nuclei will tend to form linear relationships in Ca/K two-isotope systematics, as will neutron capture on ^{40}Ca. ^{40}K is however also overproduced during spallation, relative to to both ^{41}K and ^{40}K (ref. 8); this potentially allows three isotope measurements to distinguish between cosmic ray irradiation, and *in situ* decay from initial ^{41}Ca. Indeed, the ability to resolve mass fractionation corrected ^{40}K excesses, relative to the other isotopes, may form the basis for paleo-dosimitry on meteoritic materials.

The bulk sampling/TIMS-based methods described in this paper are capable of separating K from bulk samples, and resolving 100 ppm-level K-isotope anomalies in separates containing 150 ng of K. The methods may be able to confirm or rule out the presence of ^{41}Ca in refractory inclusions at the level suggested by the SIMS-studies, uncover the former presence of ^{41}Ca in materials beyond the scope of such *in situ* methods, and may also be capable of estimating the level of cosmic ray exposure in various meteoritic materials.

2 Analytical procedures

2.1 Samples, digestion, environment and reagents

Three samples of terrestrial basalt (USGS standards BIR-1, BHVO-2 and BCR-2) were selected for analysis. These rock standards have varying matrices, K-content, Ca/K, Mg/K, Ti/K and Na/K ratios, permitting an estimation of the quality of purification. K and Ca from 1000 μg g^{-1} Alfa Aesar and K from SRM3141a metal standards was also utilized.

Samples were digested in ~0.5 mL 5/1 concentrated HF–HNO_3 at 130 °C for 2 days or longer, dried down, and re-dissolved in ~0.5 ml concentrated HCl. If any insoluble residues (most likely alkaline earth fluorides) were present, the samples were re-dried, and more concentrated HCl was added. The cycling was repeated up to 3 times, or until no insoluble residues were present. If samples didn't dissolve to form a clear solution after this repeated cycling, a small volume of saturated boric acid was added to help break down any residual fluorides. Once clear solutions were present, samples were re-dried, and converted and dissolved for loading on columns.

All sample dissolution and processing was performed in Picotrace laminar air flow benches supplied with HEPA 14 filtered air, in a clean lab environment with a separate HEPA 14 filtered air supply. All chromatographic reagents were based on sub-boiling double distilled or high purity commercial acids and waters, in order to minimize analyte-borne sample contamination. Concentrated HF utilized for sample digestion and Ti-cleanup was supplied by Seastar, HCl and HNO_3 were double-distilled inhouse from analytical grade stock, H_3PO_4 was diluted from an analytical grade stock solution, and a saturated (~1 M) solution of H_3BO_3 was made by dissolving analytical grade borate crystals in double distilled water.

2.2 K-purification

Several descriptions of ion chromatographic techniques for the separation of K have previously been published, *e.g.* AG50W-X8 cation exchange in 0.5 M $HNO_3 \pm H_2O_2$ (ref. 9, 10), 0.7 M HCl (ref. 11), and various HBr–$HClO_4$–HCl elutions on p(db)-e18-c6 crown ether (ref. 12). While AG50W-X8 resin is commonplace, the lack of a commercial polymer-supported p(db)-e18-c6 resin, in a style similar to the related Sr-spec crown ether, limits the current application of such a separation process. The described AG50W-X8 separation techniques however utilize large column volumes, *e.g.* 70 mL and 186 mL of resin, blank-wise unsuitable for small low level samples, as elution volumes and analyte blanks are correspondingly large. These chemistries must therefore be scaled to sizes more adequate for 2–4 mg refractory inclusion type sample sizes.

The primary 0.5 M HCl separation scheme developed for this study is shown in Table 1, the elution characteristics being described by the Kd table in ref. 13. A chromatographic system based on AG50W-X8 200–400 mesh cation exchange resin in 0.67 mL (0.24 cm diameter × 15 cm capillary) resin volume Teflon micro-columns was utilized. Because of the relatively high aspect ratio of the column (length/diameter), and the small mesh size of the resin, this chromatographic system is suitable for high resolution chromatography. The total exchange capacity of the resin is 1.7 meq mL^{-1} × 0.67 mL = 1.14 meq, while the charge in a HF-treated sample of refractory inclusion-like BIR-1 is ~0.024 meq mg^{-1}, resulting in a manageable resin load of ~8% if a 4 mg sample is loaded. According to INAA (instrumental nuclear activation analysis) data,[14] summarized for Ca–K in Table 2, such a 4 mg refractory inclusion sample from a reduced CV3-meteorite would typically carry *ca.* 50–200 ng K, depending on the type of inclusion, and the degree of equilibration in the meteorite from which it was recovered. The main K-cut will however also contain most of the Ti and V, as both elements more or less co-elute with K in 0.5 M HCl, Ti in particular being a significant component in refracrory inclusions. An additional separation was therefore added, where half the sample from the initial potassium separation was loaded on a Biorad column with 1 mL AG50W-X8 200–400 cation exchange resin in 0.5 M HCl, and 2 mL of 1 M HF was utilized to wash of Ti and V. The remaining Ti + V-free sample was unloaded with 6 M HCl. The Ti-dirty and Ti-cleaned samples were run separately.

Table 1 Main K separation and optional Ti cleanup

Eluent	Vol.[a]	Elements eluted
Step 1: Main K-separation[b]		
0.5 M HCL (conditioning)	2	
Load sample in 0.5M HCl	0.5	
0.5 M HCl	5.5	Cr + Li + Na
0.5 M HCl	6.5	K + Ti + V
6 M HCl	6.5	Remaining matrix
Step 2: Optional Ti-cleanup[c]		
0.5 M HCl (conditioning)	2	
Load sample in 0.5 M HCl	0.5	
1 M HF	2	Ti + V
6 M HCl	5	K

[a] Volume of eluent (mL). [b] Savillex Teflon microcolumn with 0.67 mL of Biorad AG50W-X8 200–400 mesh resin, 15 cm resin bed height. [c] Biorad-type column with 1 mL of Biorad AG50W-X8 200–400 mesh resin.

View Online

Table 2 Predicted ^{40}K and ^{41}K excesses in CV3^{reduced} refractory inclusions, and predicted initial solar system deficit[a]

Refractory inclusion	Inclusion type	Ca, μg g^{-1}	K, μg g^{-1}	Radiogenic excess ^{41}K, ppm	Ancient excess ^{40}K (%)	Recent excess ^{40}K (%)	1 Myr exp ^{40}K, ppm	4 Myr exp ^{40}K, ppm	10 Myr exp ^{40}K, ppm
Leoville 1	CTA	280000	31.7	1855	8.5	107	82	328	820
Leoville 2	B2	179000	47.4	792	3.6	46	55	219	548
Leoville 3	Finegrained	92200	30.5	633	2.9	37	85	341	852
Leoville 4	FTA	244000	18.4	2781	12.7	160	141	565	1412
Leoville 5	B2	234000	23.4	2097	9.6	121	111	444	1110
Efremovka 1	CTA	270000	11.3	5004	23	289	230	920	2299
Efremovka 2	CTA	295000	35	1765	8.1	102	74	297	742
Efremovka 3	CTA	219000	41.3	1112	5.1	64	63	252	629
Vigarano 1	B2	187000	86	454	2.1	26	30	121	302
Vigarano 2	B1	222000	20.4	2281	10.4	132	127	509	1274

Reservoir		μg g^{-1} Ca	μg g^{-1} K	Deficit ^{41}K, ppm
T_0 ^{41}K deficit	Solar	9280	558	−3.5

[a] CTA = Compact type A, FTA = Fluffy type A. The elemental compositional data are bulk INAA data,[14] the predicted radiogenic ^{41}K bulk excesses are based on the refractory inclusion ^{41}Ca/^{40}Ca ratio of ~1.41 × 10^{-8} (ref. 1), the cogenerated spallogenic ^{40}K excesses are calculated based on a ^{40}K/^{41}K production ratio of ~1 suggested in iron meteorites[8] and ^{40}K $T_{1/2}$ of 1.248 Gyr, and an ancient cogeneration age of 4.567 Gyr. The predicted recent irradiation overprints are based on a cosmogenic nuclide production rate of 5 × 10^{12} atoms kg^{-1} Myr^{-1}.

Published on 11 November 2010 on http://pubs.rsc.org | doi:10.1039/C0JA00067A
Downloaded by New Copenhagen University on 26 February 2011

2.3 Predicted isotopic patterns of meteoritic K

The expected radiometric and possible spallogenic bulk anomalies can be calculated using published data, and the anomaly levels used as a minimum target for the reproducibility of the mass spectrometry. The calculated anomalies are shown in Table 2. Using stable Ca and K isotope data,[15] the ^{41}Ca/^{40}Ca at the time of canonical refractory inclusion formation,[1] and Ca and K bulk refractory inclusion elemental concentrations,[14] the range of expected radiogenic ^{41}K excess in a suite of refractory inclusions is calculated to be ~500 ppm to 5000 ppm, relative to a terrestrial composition. Conversely, if one assumes an approximately chondritic Ca/K ratio for the solar system,[16] and isotopic homogeneity for Ca and K, an initial ^{41}K deficit at the time of refractory inclusion formation relative to the current ratio can be calculated. This initial solar system ^{41}K deficit, relative to a chrondritic composition, is only ~−3.5 ppm. This would be the expected deficit in a solid created and isolated at the time of refractory inclusion formation with a Ca/K ratio of 0, one of the earliest plausible times, and the most extreme fractionations possible. Even such an ideal depletion anomaly of −3.5 ppm would be hard to resolve, essentially emphasizing the simple observation that while excesses of ^{41}K generated by the *in situ* decay of ^{41}Ca can be highly amplified by extreme Ca/K enrichment, the same is not the case for depletions and accompanying radiogenic deficits at the ^{41}Ca-levels suggested by SIMS.

With respect to resolving an anomaly created both by an ancient and a recent *in situ* irradiation scenario, it would seem that any irradiation capable of creating the positive anomalies observed in ^{41}K, would be accompanied by a much larger cogenerated excess in ^{40}K. Such ^{40}K excesses lead to anomalous ^{40}K/^{39}K ratios, that may propagate artificial apparrent ^{41}K deficit approximately twice the size of the ^{40}K excess into the mass fractionation corrected ^{41}K/^{39}K, if the ^{39}K/^{40}K ratios is utilized for normalization. The predicted ancient and recent overprint excesses in ^{40}K shown in Table 2 are based on a ^{40}K/^{41}K production ratio of 1, such as is found in iron meteorites,[8] taking into account the higher ^{40}K at the time of refractory inclusion formation, with a ^{40}K $t_{1/2}$ of 1.248 Gyr, and an age of 4.567 Gyr for the ancient overprint. The ancient predicted ^{40}K excesses are ~2% to 23%, while the recent excesses are ~12 times higher, at ~26% to 290%. A recent meteoroid phase origin of excess ^{41}K, and hence the scenario with the highest level of cogenerated ^{40}K anomalies, can probably be ruled out, as it is hard to explain the apparrent ^{41}Ca equivalence between refractory inclusions from meteorites of varying exposure histories, and why coaccreated refractory inclusions showing no apparrent ^{41}Ca excess would escape such meteroid phase overprint.[2] Provided that the recent cogeneration scenario can be ruled out, the determination of ^{40}K anomalies thus provides a convenient method to examine ancient spallation-overprint in general as the possible source of excess two-isotope measured ^{41}K, as no other history or relevant mechanisms would seem able to return such large negative three-isotope determined ^{41}K anomalies.

The interpretation of ^{40}K-excesses, and the basic determination of possible radiogenic ^{41}K excesses, is however complicated by the possibility of overprints during both an ancient pre-accreation and a recent meteroid phase exposure. Both ancient and recent overprints may have created ^{40}K excesses that mask any primary radiogenic ^{41}K excesses measurable by three isotope analysis, and irrespective of the presence of ^{41}K excesses, the exact interpretation of any ^{40}K excesses is complicated by the possibility of a two-stage irradition history. The higher sensitivity towards recent ^{40}K overprints means that these can occur with less impact on the actual ^{41}K excess. The recent irradiation overprints in Table 2 are based on a general cosmogenic nuclide production rate of 5 × 10^{12} atoms kg^{-1} Myr^{-1}. The predicted ^{40}K excesses for a meteroid phase overprint are calculated for 1 Myr, 4 Myr and 10 Myr, corresponding to the approximate estimated exposure ages of the Murchison, Allende and Efremovka meteorites, the meteorites in which refractory inclusion-borne

 This journal is © The Royal Society of Chemistry 2011

View Online

Published on 11 November 2010 on http://pubs.rsc.org | doi:10.1039/C0JA00067A
Downloaded by New Copenhagen University on 26 February 2011

radiometric ^{41}K excesses are suggested by SIMS-analysis.[2] It can be seen that the expected generated ^{40}K excesses are much smaller than those generated by any ^{40}K + ^{41}K cogeneration scenario, indicating that ^{40}K excesses at the 1% level and above in refractory inclusions are probably not primarily meteroid phase generated. However, the predicted ^{40}K excesses in the longest 10 Myr exposure class considered, including the otherwise pristine and often utilized Efremovka meteorite, are of a size sufficient to artificially mask any radiogenic ^{41}K excesses, as determined by three isotope analysis. The possible implication is that they may no longer be used for early solar system ^{41}Ca/^{41}K three K-isotope studies.

For the above mentioned scenarios, several important caveats must however be stressed. It should be noted that an iron meteorite matrix is very different from a refractory inclusion with respect to possible target nuclei, that the rate of ^{40}K generation during meteroid phase exposure is not known for CAI-material, and that the degree of shielding that refractory inclusions experienced during their pre-accreation stage would also be drastically smaller or literally nonexistant, as compared to any meteoroid phase geometry. Finally, it is also possible that anomalous K-isotope compositions were inhereted from the K in the refractory inclusion forming environment, given the nucleosynthetic environment indicated by the apparrent presence of spallogenic ^{10}Be in many inclusions,[17] perhaps necessitating the use of internal isochrones rather than simple models when studying Ca/K three isotope systematics.

2.4 Theoretical precision on Faraday channels

As it is one of the novel elements of the analytical method, the theoretical characteristics of a 10^{10} Ω, 10^{11} Ω and 10^{12} Ω mix of resistors, with respect to noise levels and application to K-isotope measurements, merits description. Error on precision during ion beam measurement stems from Johnson-Nyquist (JN) noise emanating from blackbody radiation internal to the resistor, and Poisson noise originating from the discrete nature of the particles in the ion beam. Considering the abundances of the K-isotopes, it is clear that the largest potential noise-component, both with respect to JN and Poisson noise, is to be found in the measurement of ^{40}K, as this isotope is by far the least abundant. When applied to operational amplifiers, the resistor noise level is described by the JN equation,

$$\delta V_{\mathrm{JN}} = \sqrt{4 \times K_{\mathrm{b}} \times R \times T_{\mathrm{k}}/T_{\mathrm{s}}}$$

where δV_{JN} is the 1 s.d. JN-noise in V, K_{b} is the Stefan Boltzman constant, R is the resistor value in Ω, T_{k} is the temperature in kelvin, and T_{s} is the integration time in seconds. While the noise level measured in volts increases and scales with $\sqrt{R}$, the signal gain scales directly with R, such that the signal/noise ratio scales and improves with $\sqrt{R}$; therefore, a 10^{12} Ω resistor theoretically has a $\sqrt{10}$ times better signal/noise ratio than a 10^{11} Ω at a given intensity, with respect to JN noise.[18] The improvement in signal/noise ratio comes at the expense of decreased upper dynamic range, as the associated electronics have a limited voltage range, and the absolute voltage scales directly with resistor value.

The Poisson noise component, which becomes increasingly important at higher intensities, is simply equivalent to 1 s. d. $= 1/\sqrt{N}$, where N is the number of counted ions. When combined with Ohms law, and applied to operational amplifiers and ion current measurements in mass spectrometry, the Poisson noise level in a 1 s measurement is given by

$$\delta V_{\mathrm{P}} = \sqrt{V_{\mathrm{signal}} \times R \times e}$$

where δV_{P} is the 1 s.d. Poisson-noise in V, V_{signal} is the voltage measured, R is the resistor value in Ω, and e is the elementary charge. The combined noise level from the two componnents in a 1 s integration can be calculated by simple error propagation, as they are uncorrelated, such that

$$\delta V_{\mathrm{combined}} = \sqrt{4 \times K_{\mathrm{b}} \times R \times T_{\mathrm{k}} + V_{\mathrm{signal}} \times R \times e}$$

while Poisson noise is a fundamental continuity or quantum noise, which is determined by the total number of ions counted, and not the rate at which they are counted, JN noise accumulates over time. Part of the analytical challenge of optimal isotope ratio mass spectrometry, particularly evident in the measurement of high isotope elements such as K, is thus to measure at high enough intensities that a measurement is not unnecessarily contaminated by JN noise, and that an analysis is primarily describing inherent and essentially unavoidable quantum noise. The voltage at which the cross-over between the two regimes takes place can be calculated from combining the aforementioned equations, such that

$$V_{\mathrm{crossover}} = 4 \times K_{\mathrm{b}} \times T_{\mathrm{k}}/e$$

As can be gathered from the equation, the actual crossover voltage is independent of the resistor value, and solving for room temperature gives ~100 mV. However, since the current required to generate such a voltage is ten times lower on a 10^{12} Ω compared to a 10^{11} Ω, the crossover level scales directly with the resistor value, and occurs at lower currents on higher value resistors. Thus, on 10^{11} Ω resistors at near room-temperatures, poisson noise overtakes resistor noise at an ion current of ~10^{-12} A; on 10^{12} Ω resistors, this crossover occurs at ~10^{-13} A. This is not in agreement with ref. 19, who states that the thermal Johnson-Nyquist (JN) resistor noise present in a 10^{11} Ω resistor is equivalent to the Poisson noise in an ion current of ~8×10^{13} A, or 80 mV on a 10^{11} Ω resistor.

The observation of the flat crossover-level allows for a few simple rules of thumb, here applied to systems at approximately room temperature. When working with a analogue-digital converter capable of 10 V (Sector 54 or Isoprobe) or 50 V

Table 3 Theoretical 1 s.d. noise levels, 1 s integration[a]

Isotope and resistor	^{39}K, 10^{10} Ω	^{40}K, 10^{12} Ω	^{41}K, 10^{11} Ω
Signal	300 V	38 mV	22 V
JN-noise	130 μV	13 μV	41.3 μV
Poisson noise	2190 μV	24.7 μV	594 μV
JN-noise, ppm	0.4	344	1.9
Poisson noise, ppm	7.3	649	27
Combined noise, ppm	7.3	734	27

[a] The voltages are corrected to be equivalent to a 10^{11} Ω channel. Although these are not the actual voltages in non-10^{11} Ω channels, this is convention for reporting in mass spectrometry. The amplifier temperature utilized for the calculation was 36 °C = 309 K.

View Online

Published on 11 November 2010 on http://pubs.rsc.org | doi:10.1039/C0JA00067A
Downloaded by New Copenhagen University on 26 February 2011

dynamic range (Triton or Neptune), monotone resistors allow for measuring isotope ratios of up to 100 or 500, with the least abundant isotope in the poisson regime, as 10 V or 50 V of the major will give 100 mV of the minor. Decade resistor separation allows a ratio increase to 1000 and 5000 respectively, while two decade separation theoretically allows 10000 and 50000 ratio measurements to be conducted. With a $^{39}K/^{40}K$ ratio of ~8000, poisson regime measurements thus requires 2 decade separation. When utilizing a Triton TIMS, measuring at ~300 V ^{39}K (10^{11} Ω equivalent) on a 10^{10} Ω to allow for intensity fluctiation, gives a ~38 mV ^{40}K beam (10^{11} Ω equivalent), corresponding to an actual voltage of ~380 mV on a 10^{12} Ω, comfortably in the Poisson regime. Calculated noise levels are shown in Table 3. Measuring at higher intensities also allows for a decrease in the fraction of beam-time utilized for baseline measurements, from an optimum of ~50% in the JN-noise dominated regime, to increasingly lower fractions as the measurement moves further into the Poisson regime, and additionally allows for a faster sample throughput, as the sample is consumed and isotopically described faster.

2.5 Mass spectrometry

In order to improve the signal/noise ratio of the ^{40}K signal, according to the theory described in the section on noise on Faraday channels, the samples were measured in static mode at comparatively high intensities, with a combination of 10^{10} Ω, 10^{11} Ω and 10^{12} Ω resistors, on a Thermo-Finnegan Triton TIMS. The collection scheme is shown in Fig. 1. Samples were slowly heated to ~1 A filament current over the course of 1/2 an hour. At 1 A, the line of sight-valve was opened, the ^{39}K beam was acquired and focused, and the sample was heated and trimmed. This trim and heatup took ~10–15 min, depending on loading peculiarities. Once ^{39}K ion beam intensities were at ~300 V, the data collection was initialized. The method statically collected blocks with 128 s of K-isotope beam and 100 s of defocused electronic baseline, according to the noise levels predicted by the theory presented in section 2.5, this should yield a block precision of *ca.* 360 ppm 2 s.d. on $^{41}K/^{39}K$, utilizing exponential mass fractionation correction. The aiming window was ±3% on ^{41}K, and wheel and electrostatic focusing was performed every 5th and 10th block, respectively. Baseline delays were 10 s, in order to allow for the relatively slow decay on the 10^{12} Ω amplifier tasked to the ^{40}K beam, while setling times were 3 s, to allow the Faraday signal to rise.

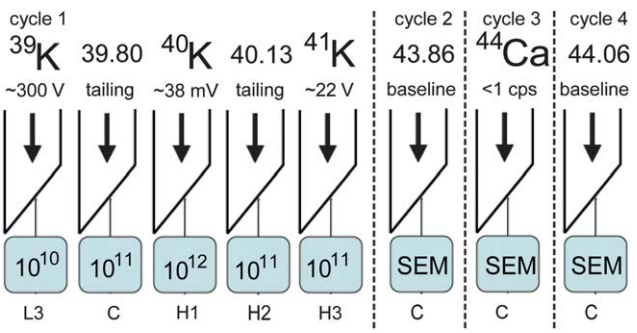

Fig. 1 Collection scheme. In addition to the K-isotope measurements, the axial SEM was used to monitor ^{44}Ca for 4 s, with 2 × 2 s baseline measurements at ±0.1 amu.

The analytical method measured at ^{44}Ca for 4 s with the axial SEM ion counter, with additional 2 × 2 s baselines at ±0.1 amu at ^{44}Ca, in order to monitor for potential ^{40}Ca isobaric interference on the ^{40}K signal. The added baseline bracketing for ^{44}Ca with the SEM was necessary, because the tailing from the high intensity ^{39}K and ^{41}K beams could generate ~0.5 counts per second in the mass 44 region. This monitoring was conducted every block, after the K-isotope measurements had taken place. Cycle-level monitoring was not utilized, because of the associated loss of beam time while waiting for SEM/Faraday switching and rise time.

The level of ^{39}K + ^{41}K tailing onto ^{40}K was monitored during analysis, by placing and measuring with Faraday cups equipped with 10^{11} resistors at ~± 0.16 amu relative to the cup tasked to the ^{40}K beam. These positions were the closest possible with the Triton geometry and standard mass dispersion. The difference between the two signals, and the purely electronic baseline, was related to the intensity of the ^{40}K beam. No correction was carried out, as this would significantly degrade the precision level through error propagation from the 10^{11} resistors. Samples would generally run 3–10 h uninterrupted until filament exhaustion, except for particularly low-yielding samples, as will be expanded on.

2.6 Data reduction

Data reduction was carried out offline in Microsoft Excel, and the isotopic ratios and atomic weight data were derived or taken from a compilation of abundance and weight data.[15] The isotopic abundances, masses and the resulting ratios and mass fractionation correction exponents are shown in Table 4. Generally, instrumental TIMS and natural mass fractionation is expected to follow kinetic rather that an equilibrium behaviour, best corrected by the exponential law.[20,21]

The high intensity rock standard data was subjected to a theoretical signal/noise ratio-based assesment, in order to avoid

Table 4 Key isotope parameters[a]

Isotope	^{39}K	^{40}K	^{41}K
Mass	38.9637	39.96400	40.96183
Abundance	0.932581 ± 29	0.0001167 ± 4	0.067302 ± 29
Estimated error	~31 ppm	~3600 ppm	~430 ppm
Ratio	$^{40}K/^{39}K$	$^{41}K/^{39}K$	$^{40}K/^{41}K$
Mole ratio	0.00012516 ± 45	0.072168 ± 31	0.0017343 ± 62
Estimated error	~3600 ppm	~450 ppm	~3600 ppm
Exponent	**Exponential**	**Rayleigh**	**Equilibrium**
$^{41}K/^{39}K$–$^{40}K/^{39}K$	1.97290	1.96081	1.94887
$^{40}K/^{39}K$–$^{41}K/^{39}K$	0.506868	0.509992	0.513117

[a] Masses, isotopic abundances and abundance uncertainties are from ref. 15. Abundance ratios, propagated abundance ratio errors, and correction exponents are based on these data.

 This journal is © The Royal Society of Chemistry 2011

View Online

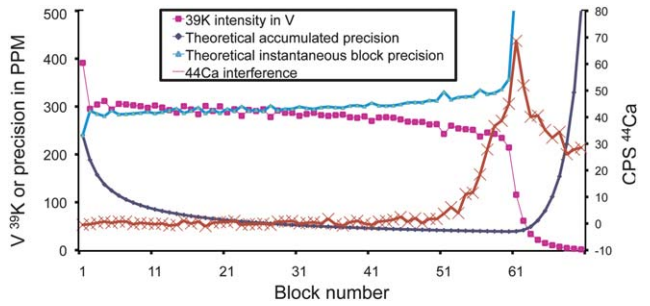

Fig. 2 Beam evolution for an example analytical run of a Ti-dirty BHVO-2 sample.

the inclusion of low intensity/precision data. The theoretical level of precision for each block was calculated based on the formulae in section 2.3, and the intensity of the ion beam. Based on this, it was calculated whether a block would statistically enhance or degrade the precision of the analytical run. An example run is shown in Fig. 2. The instantaneous block precision shows the theoretical 2 s.d. precision level for each individual block in ppm on $^{41}K/^{39}K$ ratio with exponential mass fractionation correction, and is anticorrelated with the beam intensity. The accumulated precision traces the calculated 2 s.e. theoretical precision on the $^{41}K/^{39}K$ ratio for the entire analytical run, up to and including that block. According to the utilized method, blocks collected after the inflection point on the accumulated precision at block 61 of this run are not included in the final data reduction, as the theoretical precision would be lower. This is not classical outlier rejection, as the rejection was carried out regardless of the actual mass fractionation corrected value of the block, but rather a method for avoiding the inclusion of low precision data in the final data reduction. No such outlier rejection was utilized.

In most long sample runs of 150 ng with 80 or more blocks, the low precision condition was generally only encountered close to filament exhaustion, with blocks showing less than ~25 mV ^{40}K; for small loads of 10 ng of 5–10 blocks, where the dilution of precision would be less severe for a low intensity block, the cutoff level was generally lower, at ~15 mV. The blocks rejected by this method were generally only the last 1 or 2 blocks collected before the filament completely depleted to a ^{39}K intensity below 1 V. Blocks showing more than 1 CPS of ^{44}Ca, corresponding to an interference level that would generate an artificial 50 ppm deficit in $^{41}K/^{39}K$ ratio, were also removed from the data-set, this condition being met at block 50 in the example run (Fig. 2) of a Ti-dirty sample BHVO-2 sample. It can however be seen that there are indication of some Ca-interference before this condition was encountered, these conditions were only rarely encountered for Ti-cleaned samples.

3 Results and discussion

3.1 Chemical yields and blanks

Quantitative recovery during column separation is particularly important for relatively low-mass elements, as isotopic fractionation during column chemistry can assume an equilibrium behaviour, generating artificial anomalies if an exponential correction assuming kinetic behaviour is utilized for mass fractionation correction.[22] Considering the differences in the mass fractionation correction algorithms, it can be calculated that a 1‰ fractionation in $^{39}K/^{40}K$ by an equilibrium law, rather than a exponential law, will lead to an artificial mass fractioned $^{41}K/^{39}K$ anomaly of ~24 ppm if corrected by the exponential law. The expected content in the rock standards, and the actual yields, are listed in Table 5. The content in the separates was determined by isotope dilution with a ^{39}K spike. Chemical yields were in the range 95–100% for K, relative to the reported and certified values for the geostandards. These yields are quantitative or near-quantitative.

Table 5 Chemical yield during potassium separation[a]

Rock Standard	Expected, ng K	Recovered, ng K	% Yield
BIR-1, (1)	1000 ± 100	1060 ± 50	~100%
BIR-1, (2)	1000 ± 100	1060 ± 50	~100%
BHVO-2	17800 ± 420	17600 ± 350	~99%
BCR-2	52800 ± 1400	50200 ± 1000	~95%

[a] Compositional data are the rock standard certified values, uncertainties are 2 s.d., blanks were typically 100–200 pg K.

The blanks were typically on the order of 100–200 pg, likewise determined by isotope dilution with a ^{39}K spike. For single 150 ng K samles, this corresponds to a neglible blank of ~1‰ of the sample size, while it becomes a quite significant component of a 10 ng sample. This may be particularly problematic if the isotopic contrast between the sample and the contaminant is considerable, as would be expected in the case of refractory inclusions.

3.2 Initial TIMS loading technique experiments

To support long-lasting, high ion current measurements on small K samples, various loading techniques were tested with respect to yields and filament blank levels. Because of the problem of Ca-interference and ^{39}K + ^{41}K tailing onto the minor ^{40}K isotope beam, ^{40}Ca interference and abundance sensitivity were given special attention during testing. K from a 1000 μg g^{-1} 5% HNO_3 plasma standard (Alfa Aesar) was converted/dried down to the appropriate chloride or nitrate form, taken up in 0.5 HCl or 0.5 M HNO_3, and loaded for analysis on filaments. 50 ng of K was utilized for the initial experiments. If additional loading reagents were utilized, these were added to the filament subsequent to sample drydown. Ta, W and Re single filaments were tested, as were Re double filaments. Loading acids or mixes were HCl, HNO_3, H_3PO_4, H_3BO_3, Ta-activator with H_3PO_4, and Si-gel. The most promising loading techniques were subjected to an extended test with 100 ng synthetic standard loads, and an early development of the high precision method, before the final loading technique used for rock standards was decided upon.

Re double filaments gave yields in the 5% region, but exhibited considerable Ca-interference, most likely because the high temperatures on the ionization filament gave a relatively high sensitivity towards Ca emanating from the sample/evaporation filament, and because the ionization filament itself continuously emitted Ca. This could generate several hundred counts per second at ^{44}Ca, more than could accurately be corrected by SEM ion counting. Although this interference may have been mediated

Downloaded by New Copenhagen University on 26 February 2011
Published on 11 November 2010 on http://pubs.rsc.org | doi:10.1039/C0JA00067A

View Online

Published on 11 November 2010 on http://pubs.rsc.org | doi:10.1039/C0JA00067A
Downloaded by New Copenhagen University on 26 February 2011

by running the ionization filament at lower temperature, or by conducting a more thorough filament out-gassing, the double filament technique was abandoned, as it was apparrent that it yieldwise underperformed relative to the best single filament methods.

Re single filaments did not yield high intensity beams for any significant amount of time with any of the tested loading solutions, and yields in HCl, HNO_3 and H_3BO_3 were also low for Ta. H_3PO_4, Ta-act + H_3PO_4 and Si-gel gave high yields in the 20–45% range with single Ta filaments, but indications of slightly higher tailing from ^{39}K and ^{41}K in Ta-activator + H_3PO_4 led to its initial abandonment. W filaments required a special loading technique, where the heated filament was dabbed with parafilm prior to loading. This had the effect of limiting the spread of the sample solution during loading, a problem that was present on all W filaments, regardless of aging. W filaments run without this procedure would only give low yields in the 1–4% range, while parafilm-treated filaments would yield similar to the best Ta loading techniques with H_3PO_4. The parafilm-treated W-filaments were checked for filament blanks, and although these were not considerably higher than the Ta-filaments with *ca.* 2 pg blanks, any mishandling of parafilm could potentially result in much higher blanks. Because of the added complexity and potential for contamination from the parafilm, W filaments loading techniques were not pursued. In order to discern which of the loading solutions was optimal on Ta-filaments, the H_3PO_4 and Si-gel loading techniques were subjected to extended tests, with an early version of the high precision method. The tests indicated that H_3PO_4 gave slightly enhanced yield, precision and accuracy, as compared to Si-gel. There was no difference between the nitrate and chloride forms loaded in phosphoric.

At face value, the results of these yield tests are surprising, considering the theory of surface ionization. According to the Saha-Langmuir equilibrium equation for surface ionization, filament materials with high work-functions should yield higher ionization fractions than low work-function materials. This behavior was however not found during yield experiments, as Ta-filaments (eV = 4.25) and parafilm treated W (eV = 4.55) clearly outperformed Re-filaments (eV = 4.96), perhaps indicating that ionization in a TIMS is not an equilibrium surface ionization process. However, the highest yields were achieved on Ta filaments aged for approximately 1 month subsequent to outgassing. Completely fresh Ta-filaments would not yield high intensity beams for any significant amount of time, and would also exhibit the same sample-spreading effect found with W. The improvements with aged filaments most likely stems from the formation of an oxidized surface layer, either resulting in a smaller and more easily focusable sample deposit subsequent to drydown, or through some mechanism of enhanced ion formation. This may also be the explanation for the high ionization yields on Ta as compared to other nominally higher work function metals, as Ta-oxide is reported to have an electron work-function of ~6 eV, higher than any of the tested metals.

3.3 Abundance sensitivity tests

In order to estimate the tailing in the mass 40 region, A SEM-based ~30 min 300 step mass scan was conducted at ~40 V ^{39}K and ~310000 cps ^{40}K, the resulting mass spectrum is shown in

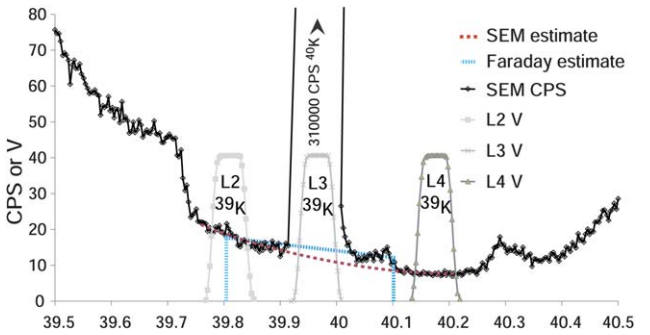

Fig. 3 SEM mass scan in the ^{40}K region at ~40 V ^{39}K and ~310000 CPS ~5 mV ^{40}K, with ^{39}K Faraday collection indicated, and SEM + Faraday-based estimates of tailing.

Fig. 3. The use of the SEM was nescessary in order to measure the low absolute level of the tailing, and the beam intensity was lowered relative to high intensity measurements, in order to avoid saturating or damaging the SEM. The L3 and H3 cups were positioned such that L3-SEM-H3 were positioned for simultaneous ^{39}K, ^{40}K and ^{41}K collection respectively, and the L2 and L4 cups were positioned as close as possible to L3, in order to collect the ^{39}K in proximity to ^{40}K collection. The signal intensity in V in the L2, L3 and L4 cups is plotted along the SEM-data in Fig. 3. The source and analyzer vacuum levels were $\sim 6 \times 10^{-8}$ and $\sim 2.8 \times 10^{-9}$, respectively, similar to the levels during high intensity measurement. It is worth noting that the SEM placement and aperture geometry remains somewhat different from that of the H1 Faraday used during actual analysis, and direct comparison with the Faraday-based data is therefore somewhat compromised, as these differences may affect the pattern and relative sensitivity towards tailing.

According to the SEM mass scan, the background generally diminishes towards the ^{40}K peak, consistent with the expected behaviour of scatter from the beams of ^{39}K and ^{41}K, but irregularities are present in the mass spectrum. Most importantly, the count level on the SEM significantly decreases during ^{39}K collection in L2 and L4, indicating that the background level when ^{39}K is transmitted but not collected is enhanced compared to the level found during collection or when the beam interacts with the Faraday. We interpret this as the result of reflections and scatter in the collector array, an effect that somewhat complicates the interpretation and estimation of the actual tailing on the ^{40}K peak during analysis. The most plausible tailing estimate would seem to be given by connecting the levels found during L2 and L4 ^{39}K collection at *ca.* 39.75–39.79 and 40.1–40.25, suggesting tailing at the 15 cps level, corresponding to *ca.* 50 ppm of the ^{40}K beam.

The level of tailing and scatter was also estimated by taking the average of measurements with Faraday cups at 39.8 and 40.13 during the initial TIMS experiments. Apart from the previously mentioned minor difference between H_3PO_4 and Si-gel, it was found that the level of tailing decreased to a level of ~60–70 ppm of the ^{40}K signal at a source vacuum level of $\sim 1.3 \times 10^{-7}$ mbar, corresponding to the typical turbopump-driven final vacuum, but only improved slightly towards 50 ppm of the ^{40}K signal at lower cold trap assisted levels as low as 4×10^{-8} mbar. This likely indicates that the analyzer and backend vacuum levels were more

 This journal is © The Royal Society of Chemistry 2011

View Online

Published on 11 November 2010 on http://pubs.rsc.org | doi:10.1039/C0JA00067A
Downloaded by New Copenhagen University on 26 February 2011

important, once the source scattering had been brought to a certain level, reflecting the short flight distance in the source compared to the analyzer. At cold trap assisted final vacuum, the signal at 39.8 was *ca.* 60 ppm of the ^{40}K, while the signal at 40.13 was *ca.* 40 ppm. These tailing estimates have been transformed to their equivalent CPS at 310000 CPS ^{40}K, and plotted on Fig. 3 alongside the SEM-scan data. The individual Faraday-based estimates are in excellent aggreement with the SEM-based measurements, although the actual Faraday tailing estimate at ^{40}K is somewhat higher than the SEM-estimate because of the non-linear nature of the tailing. These general tailing effects complicated the use of any analytical baseline measurement, and electronic baselines were therefore chosen. Any tailing during actual analysis would however remain uncorrected by an electronic baseline measurement, and any variation in relative tailing-level between samples would lead to differences in the mass fractionation corrected values, nescessitating consistent high vacuum conditions during actual sample measurement.

3.4 Tests of isobaric interferences

Test of the level of isobaric interference for the single filament H_3PO_4 loading technique were previously carried out on a Sector 54 TIMS, with a combined synthetic 2 ng Ca/10 ng K load, in order to investigate the relative sensitivity of K relative to Ca. These tests indicated a very low sensitivity towards Ca compared to K, as the counts at ^{44}Ca were 1 count per second or lower on an ion counter at ~100 V ^{39}K. This corresponds to a sensitivity ratio of $\sim 3 \times 10^7$ in the encountered K analysis envelope. Such a low relative sensitivity for Ca is not surprising, considering the refractory nature and high ionization energy of Ca compared to K. It is however worth noting that this relative sensitivity gap may not be as pronounced in actual samples, as the ionization characteristics of real samples can be very different from the tested synthetic mixture. Generally, any unseparated sample matrix will dilute the element of interest, retarding evaporation and poisoning ionization, leading to correspondingly higher filament currents and temperatures for a given ion beam intensity. Furthermore, the sensitivity gap will likely shrink during an actual analysis, as the temperature increases, and K depletes relative to the Ca.

The absolute level of Ca-interference is important, as it represents the worst-case scenario for an isobaric interference, namely that of the most abundant isotope of the antagonistic element interfering with the least abundant isotope of the element of interest. If present at sufficiently low intensities, such an interference is best corrected by a sensitive method such as secondary electron multiplier ion counting, as the secondary electron multiplier signal/noise characteristic are well suited for such applications, where their nonlinearity at high signal intensities and relative lack of dynamic range and gain stability do not represent problems. If the gain-stability related error of a secondary electrom multiplier compared to a Faraday is on the order of 1%, this would correspond to a propagation of an error of ~0.5 counts per second of ^{40}Ca for each ^{44}Ca counted. At ~38 mV ^{40}K, the number of ions per second is ~2000000, and it would require a signal of ~100 counts per second ^{44}Ca to propagate an isobaric interference correction error of $\sim\pm$ 50 ppm into the ^{41}K/^{39}K ratio. If no correction is carried out, and the ^{44}Ca is simply monitored to confirm that the interference is below a certain level, 1 count per second of ^{44}Ca would then simply generate an artificial 50 ppm deficit in ^{41}K/^{39}K ratios.

3.5 High precision standard tests

150 ng processed rock standard and SRM3141a standards were run according to the described procedures. The data is shown in Table 6 and plotted in Fig. 4. The Ti-dirty BCR-2 and BHVO-2 datasets, and the Ti-free BHVO-2 and BIR-1 datasets, ran with similar emission characteristics and yields, with a tendency for the Ti-dirty BCR-2 and the Ti-free BHVO-2 to give higher transmission yields than the Ti-dirty BHVO-2 and Ti-clean BIR-1. With respect to the Ti-dirty BIR-1 samples, only 3 of the 5 loaded samples reached stable emission patterns; one of these exhibited significant Ca-interference, and was therefore omitted from the data table. The Ti-dirty BIR-1 samples that did reach stable emission clearly underperformed with respect to yield, transmitting only ~10% to the analyzer, and required higher filament temperatures and currents required to reach a given intensity. This is most likely due to the relatively high Ti-content in the Ti-dirty BIR-1 separates, as the Ti/K ratio is ~20 in BIR-1, a ratio that will not have been significantly lowered by the 1 column separation scheme utilized for these samples. This interpretation seems to be confirmed by the data for the Ti-cleaned BIR-1 samples, which gave considerably higher yields and stable emission patterns. Ti-cleanup did apparrently not provide such large improvements for the already high-yielding BHVO-2 samples, suggesting that the presence of some Ti, even at Ti/K levels as high as the BHVO-2 ratio of ~4, is not a major problem for K-yield. The slight underperformance of the Ti-cleaned BIR-1, relative to the Ti-cleaned BHVO-2, might reflect the higher level of residual unseparated matrix or minor organics contamination from the cation resin, left relatively undiluted by the low total K content in the separate. In any case, the cleanest samples gave approximately the same yields and internal precisions as the SRM3141a standard reference material, indicating that it is possible to purify K by cation exchange chemistry to levels sufficient to avoid filament poisoning and other precision-limiting effects.

The Ti-dirty BCR-2 and BHVO-2, and the Ti-free BHVO-2 and BIR-1 datasets, generally show external reproducibilities of ~40–80 ppm on the ^{41}K/^{39}K ratio, and 20–40 ppm on the ^{40}K/^{39}K ratio, a pattern consistent with the error propagation characteristics described in the section on precision on Faraday channels. Although there are variations in the apparrent external reproducibilities between the data sets, the small scales ($n = 5$) of the individual dataset, limits the conclusions one can draw with respect to external reproducibility, apart from concluding that it is on the order of 100 ppm or better for ^{41}K/^{39}K, and 50 ppm or better for ^{40}K/^{39}K. Calculating a 2 s.d. on the 4 combined datasets mentioned above ($n = 20$) gives a 2 s.d. reproducibility of ~60 ppm for ^{41}K/^{39}K, and ~30 ppm for the ^{40}K/^{39}K. Although this is strictly speaking not a measure of external productivity as such, as the measurements were conducted on different samples, the 2 s.d. variation is probably a fair conservative estimate of the overall external reproducibility of the method for these sample sizes. The SRM3141a standards yielded external reproducibilities comparable to, and absolute mass fractionation corrected ratios within error of, the chemically processed rock standards.

View Online

Published on 11 November 2010 on http://pubs.rsc.org | doi:10.1039/C0JA00067A
Downloaded by New Copenhagen University on 26 February 2011

Table 6 150 ng and 10 ng standards, yield, precision and reproducibility tests[a]

150 ng standards	$^{41}K/^{39}K \pm 2$ s.e./*2 s.d.*	ppm	$^{40}K/^{39}K \pm 2$ s.e./*2 s.d.*	ppm	tailing (ppm)	avg. $^{39}K/V$	% yield
BCR-2 Ti-dirty 150 ng (1)	0.0722204 ± 34	53/34	0.0001251117 ± 34	27/17	40 ± 37	282	20
BCR-2 Ti-dirty 150 ng (2)	0.0722205 ± 31	43/27	0.0001251116 ± 27	22/13	40 ± 23	287	32
BCR-2 Ti-dirty 150 ng (3)	0.0722178 ± 27	37/26	0.0001251139 ± 24	19/13	54 ± 20	287	34
BCR-2 Ti-dirty 150 ng (4)	0.0722181 ± 26	36/27	0.0001251137 ± 23	18/14	35 ± 16	288	31
BCR-2 Ti-dirty 150 ng (5)	0.0722210 ± 34	47/28	0.0001251111 ± 30	24/14	46 ± 32	298	26
Average and 2 s.d.	*0.0722196 ± 30*	*41*	*0.0001251124 ± 26*	*21*	*43 ± 25*	*288*	*29*
BHVO-2 Ti-dirty 150 ng (1)	0.0722202 ± 27	38/27	0.0001251118 ± 24	19/14	48 ± 20	295	32
BHVO-2 Ti-dirty 150 ng (2)	0.0722189 ± 32	45/33	0.0001251130 ± 28	23/17	70 ± 25	285	22
BHVO-2 Ti-dirty 150 ng (3)	0.0722185 ± 33	46/29	0.0001251133 ± 29	23/14	56 ± 25	289	28
BHVO-2 Ti-dirty 150 ng (4)	0.0722253 ± 44	61/45	0.0001251073 ± 39	31/23	45 ± 32	293	18
BHVO-2 Ti-dirty 150 ng (5)	0.0722198 ± 49	68/40	0.0001251122 ± 43	34/20	56 ± 29	282	16
Average and 2 s.d.	*0.0722205 ± 55*	*77*	*0.0001251116 ± 49*	*39*	*55 ± 26*	*289*	*23*
BHVO-2 Ti-free 150 ng (1)	0.0722154 ± 35	48/30	0.0001251161 ± 30	24/15	57 ± 24	294	26
BHVO-2 Ti-free 150 ng (2)	0.0722195 ± 34	47/31	0.0001251124 ± 30	24/16	46 ± 21	298	25
BHVO-2 Ti-free 150 ng (3)	0.0722170 ± 29	40/31	0.0001251147 ± 25	20/16	46 ± 25	296	23
BHVO-2 Ti-free 150 ng (4)	0.0722215 ± 31	43/31	0.0001251107 ± 27	22/16	33 ± 23	297	23
BHVO-2 Ti-free 150 ng (5)	0.0722195 ± 30	42/29	0.0001251125 ± 26	21/15	−1 ± 21	296	27
Average and 2 s.d.	*0.0722186 ± 48*	*66*	*0.0001251133 ± 42*	*34*	*36 ± 23*	*296*	*25*
BIR-1 Ti-free 150 ng (1)	0.0722211 ± 30	41/32	0.0001251111 ± 26	21/16	45 ± 30	292	23
BIR-1 Ti-free 150 ng (2)	0.0722176 ± 31	43/42	0.0001251141 ± 27	22/21	93 ± 42	280	16
BIR-1 Ti-free 150 ng (3)	0.0722224 ± 38	53/34	0.0001251099 ± 33	27/17	57 ± 26	287	22
BIR-1 Ti-free 150 ng (4)	0.0722192 ± 41	57/34	0.0001251127 ± 36	29/17	43 ± 22	287	22
BIR-1 Ti-free 150 ng (5)	0.0722204 ± 47	65/43	0.0001251117 ± 41	33/22	46 ± 28	284	15
Average and 2 s.d.	*0.0722201 ± 37*	*51*	*0.0001251119 ± 32*	*26*	*57 ± 30*	*286*	*20*
BIR-1 Ti-dirty 150 ng (1)	0.0722225 ± 57	78/51	0.0001251099 ± 50	40/26	28 ± 53	258	10
BIR-1 Ti-dirty 150 ng (2)	0.0722204 ± 47	65/57	0.0001251117 ± 41	33/29	128 ± 89	236	8
Average and 2 s.d.	*0.0722214 ± 30*	*41*	*0.0001251108 ± 26*	*21*	*78 ± 71*	*247*	*9*
Rock 150 ng ex. BIR-1 Ti-dirty							
Average and 2 s.d.	*0.0722197 ± 43*	*60*	*0.000125112 ± 37*	*30*			
SRM 3141a 150 ng (1)	0.0722171 ± 32	44/32	0.0001251145 ± 28	22/16	51/22	300	21
SRM 3141a 150 ng (2)	0.0722195 ± 31	43/30	0.0001251124 ± 27	22/15	51/24	298	25
SRM 3141a 150 ng (3)	0.0722230 ± 38	52/38	0.0001251094 ± 33	27/19	41/33	293	16
SRM 3141a 150 ng (4)	0.0722182 ± 63	88/48	0.0001251136 ± 56	45/24	54/31	292	10
SRM 3141a 150 ng (5)	0.0722190 ± 22	30/24	0.0001251129 ± 19	15/12	53/17	302	39
Average and 2 s.d.	*0.0722194 ± 37*	*62*	*0.0001251126 ± 33*	*31*	*50 ± 25*	*297*	*22*

10 ng standards	$^{41}K/^{39}K \pm 2$ s.e./*2 s.d.*	ppm	$^{40}K/^{39}K \pm 2$ s.e./*2 s.d.*	ppm	tailing (ppm)	avg. $^{39}K/V$	% yield
BHVO-2 Ti-free 10 ng (1)	0.0722042 ± 130	180/173	0.0001251259 ± 114	91/87	28 ± 119	220	12
BHVO-2 Ti-free 10 ng (2)	0.0721974 ± 175	243/119	0.0001251319 ± 154	123/60	76 ± 100	234	26
BHVO-2 Ti-free 10 ng (3)	0.0722032 ± 178	246/142	0.0001251268 ± 156	125/72	90 ± 83	217	19
BHVO-2 Ti-free 10 ng (4)	0.0722042 ± 130	180/173	0.0001251259 ± 114	91/87	28 ± 119	220	12
BHVO-2 Ti-free 10 ng (5)	0.0722140 ± 157	217/208	0.0001251173 ± 138	110/105	94 ± 306	203	13
Average and 2 s.d.	*0.0722046 ± 119*	*165*	*0.0001251256 ± 105*	*84*	*63 ± 145*	*219*	*17*
Alfa Aesar standard 10 ng (1)	0.0722119 ± 106	146/103	0.0001251191 ± 93	74/52	67 ± 60	232	37
Alfa Aesar standard 10 ng (2)	0.0722034 ± 115	159/141	0.0001251266 ± 101	81/71	86 ± 157	274	15
Alfa Aesar standard 10 ng (3)	0.0722093 ± 122	169/110	0.0001251214 ± 107	85/56	40 ± 101	257	28
Alfa Aesar standard 10 ng (4)	0.0722154 ± 126	174/103	0.0001251161 ± 111	88/52	32 ± 64	240	38
Alfa Aesar standard 10 ng (5)	0.0722120 ± 129	179/130	0.0001251191 ± 113	90/66	3 ± 122	207	29
Average and 2 s.d.	*0.0722104 ± 89*	*124*	*0.0001251205 ± 78*	*63*	*46 ± 101*	*242*	*29*

[a] The average for the 150 ng standards excludes the Ti-dirty BIR-1 dataset. The values in the ppm-columns are arranged as "actual precision/theoretical precision" for the individual runs, while the numbers in cursive in the rows for the datasets are the external reproducibilities in ppm.

The average mass fractionation corrected $^{41}K/^{39}K$ ratio is within the albeit large error of the referenced stable $^{41}K/^{39}K$, when error propagation from the referenced $^{40}K/^{39}K$ ratio utilized for mass fractionation correction is taken into account. The mass fractionation corrected $^{41}K/^{39}K$ ratio of 0.0722197 ± 43 is higher than the stable value of 0.0721680 ± 310 calculated from the data of ref. 15, while the measured mass fractionation corrected $^{40}K/^{39}K$ ratio of 0.000125112 ± 37 is lower than the

 This journal is © The Royal Society of Chemistry 2011

View Online

Published on 11 November 2010 on http://pubs.rsc.org | doi:10.1039/C0JA00067A
Downloaded by New Copenhagen University on 26 February 2011

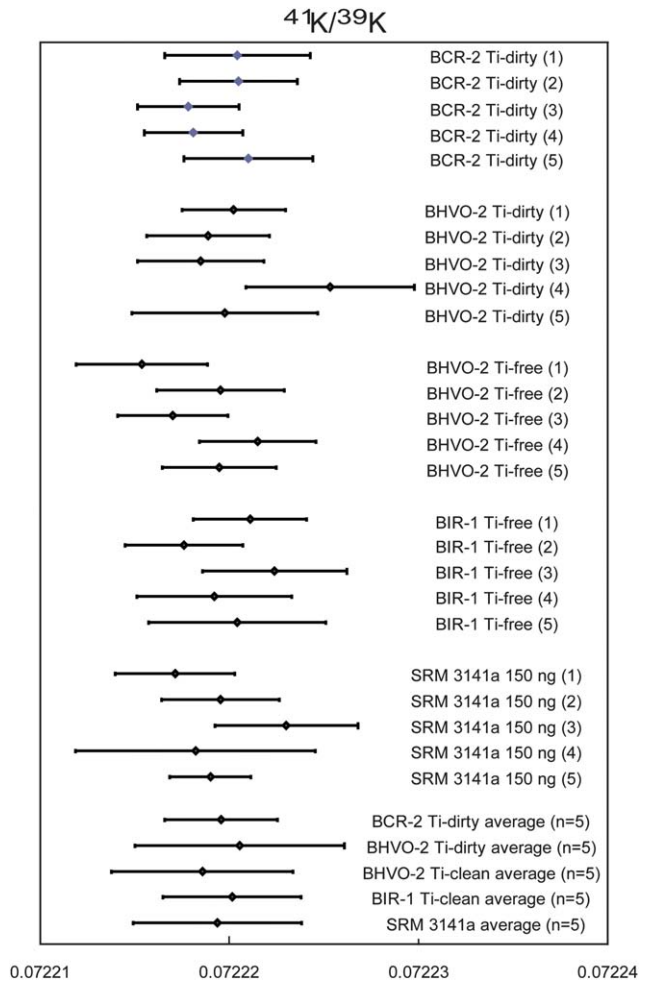

Fig. 4 High precision analyses, 150 ng samples. Error bars are 2 s.e. internal precision for individual samples, 2 s.d. for data set averages.

published ratio of 0.00012516 ± 45; indeed, the real ratio may be lower still, considering the apparrent $^{39}K + ^{41}K$ tailing component in the ^{40}K signal. The most likely explanation for these results is an overestimation of the ^{40}K in natural K, as ^{40}K is the lowest level isotope, and hence the most difficult to measure. This is indicated by the ~3600 ppm error on the ^{40}K mole fraction estimates, compared to the ~30 ppm and ~430 ppm errors on the ^{39}K and ^{41}K mole fractions, respectively. In this three isotope space, a correction of the $^{40}K/^{39}K$ isotope ratio used in mass fractionation correction of $^{41}K/^{39}K$ to the $^{40}K/^{39}K$ value found from the mass fractionation corrected $^{40}K/^{39}K$ would automatically correct the apparrent stable $^{41}K/^{39}K$ mismatch. This value is within the uncertainty range of the referenced $^{40}K/^{39}K$ ratio, and the resulting error estimate would be significantly lower, as the main determining factor would then becomes the uncertainty on the stable $^{41}K/^{39}K$. However, considering the remaining 450 ppm uncertainty on the published $^{41}K/^{39}K$ value itself, and our lack of measurements on the certified SRM 985 isotopic standard on which the prior measurements were conducted, we are not currently suggesting a revised ^{40}K abundance.

The suggested level of tailing from the major $^{39}K + ^{41}K$ beams onto the minor ^{40}K beam was systematically monitored by Faraday cups at 39.80 and 40.13, and the simple average of these measurements suggest a significant tailing component from the major $^{39}K + ^{41}K$ beams onto the minor ^{40}K beam on the order of ~40–60 ppm, such as was found during method development. Because of the use of separate detectors to monitor the tailing, as opposed to simply using analytical baselines, any attempt at correcting the ^{40}K beam measurements with these separate cups will propagate significant resistors noise into the already precision-limiting ^{40}K measurement. As can be seen from the data, the 2 s.e. precision on the tailing estimate is on the order of the precision on the mass fractionation corrected $^{40}K/^{39}K$ measurement, indicating that the penalty on the precision would be an increase in the error on the order of $\sim\sqrt{2}$. Regardless of a possible variation in tailing, the reproducibility on the 150 ng test reach the level required for *e.g.* ^{41}Ca studies in refractory inclusions. The tailing may however contribute to the underperformance of the external reproducibility relative to the internal precision, for the measured sample sizes of 150 ng K, and these abundance sensitivity related issues may present a barrier that must addressed in order to further improve the external reproducibility.

3.6 Instrumental mass fractionation

An linearized plot of the three isotope evolution during the analysis of a Ti-cleaned BHVO-2 sample is shown in Fig. 5. The mass fractionation correction exponent suggested by a regression analysis on these raw isotope data is −1.958 ± .003 2 s.e., distinct from exponential exponent of 1.9729 utilized for the actual correction. The average correction exponent suggested by data reduction on all the data-sets is ~1.961, an exponent similar to the Rayleigh fractionation correction exponent, and the data are marginally more precise and reproducible with a Rayleigh mass fractionation correction. This suggest that the reservoir mass fractionation during TIMS analysis of K may actually follow a Rayleigh type behaviour. However, as the refractory inclusions target material that the method is developed for may have experienced a large natural mass fractionation, most likely following an kinetic behaviour described by the exponential law rather than the Rayleigh law,[21] data reduction utilizing the Rayleigh exponent on such samples may introduce artificial anomalies. Considering the small impact on internal precision

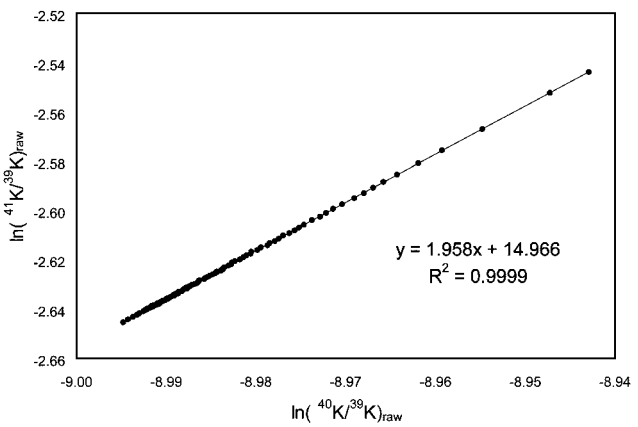

Fig. 5 Linearized K-isotope evolution for a Ti-free BHVO-2 analysis. Least squares regression output is shown in the graph.

View Online

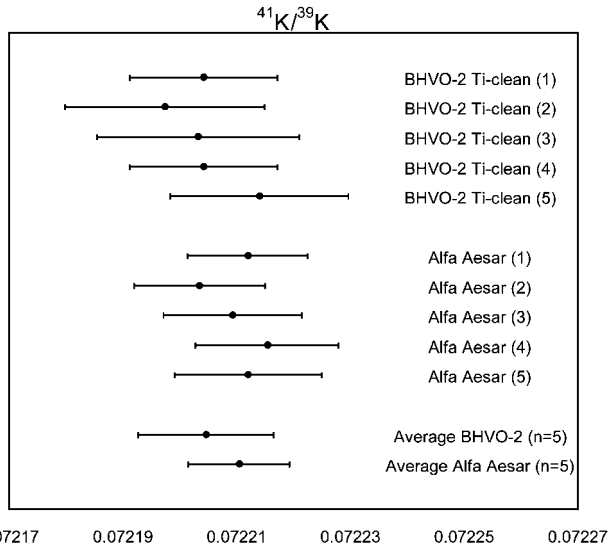

Fig. 6 Analysis of 10 ng standards. Error bars are 2 s.e. internal precision for individual samples, 2 s.d. for data set averages.

and external reproducibility caused by mass fractionation correction with the exponential law, the exponential law is provisionally recommended for correction. It is however nescessary to stress the importance of achieving filament exhaustion if there is any indication that the instrumental mass fractionation is not properly correctly described by the utilized fractionation law, as filament exhaustion provides a form of symmetrical miscorrection on samples, counteracting the effects of the offset in instrumental mass fractionation correction.

3.7 Small standard tests

10 ng rock standard and synthetic samples were run according to the described procedures. The data is shown in Table 6 and plotted in Fig. 6. While the internal precision and external reproducibility-level of ~100–150 ppm on $^{41}K/^{39}K$ reached during analysis of these small samples is lower than the level found during analysis of the 150 ng samples, the method scales well to these sizes. There is however a significant offset of the measured values towards lower $^{41}K/^{39}K$ and higher $^{40}K/^{39}K$ ratios, perhaps reflecting a non-linear response of the amplifier curcuits. Because of the smaller sample size, the ion currents reached during actual data collection are somewhat lower than those found during analysis of the larger 150 ng samples, as the samples would deplete at a rate sufficient to cause significant intensity drops between ion beam intensity adjustments and data collection. This may have caused a non-linear offset in amplifier gain, as compared to the stable higher intensity measurements conducted on the 150 ng samples.

3.8 Precision level

As can be seen from the calculation of the actual internal precision, and the calculated theoretical internal precision based on the combined JN and poisson noise, the actual precision achieved during the high intensity measurements falls somewhat short of the calculated theoretical level. For the 150 ng data-sets, the internal precision levels on $^{41}K/^{39}K$ ratios are at the 40–50 ppm level, while the levels on the $^{40}K/^{39}K$ ratios are at the 20–25 ppm level; however, the calculated theoretical precision levels are at the 30–45 ppm level for the $^{41}K/^{39}K$ ratio and 15–20 ppm level for the $^{40}K/^{39}K$ ratio. Similar underperformance is found for the 10 ng standards. The cause of this underperformance is most likely excess noise in the ^{40}K measurement on the 10^{12} Ω Faraday channel, as this is the most sensitive component. Some loss of precision also arises from the use of an exponential rather than a Rayleigh type mass fractionation correction, but a fundamental underperformance remains, even with an adjusted mass fractionation correction. Because of the straightforward nature of Poisson noise, it can be deconvolved from the overall precision, to leave a residual component containing JN-noise and any excess noise component. Such a calculation indicates that the internal precision level in the best analytical runs is consistent with the presence of noise equivalent to JN-noise at the level found in a $\sim 10^{11.7}$ Ω resistor instead of a 10^{12} Ω; such a significant underperformance relative to theory has already been reported.[18]

4 Conclusion

In summary, the combination of high yield, high intensity, high abundance sensitivity and low interference allows for relatively straightforward ~60 ppm level $^{41}K/^{39}K$ and ~30 ppm level $^{40}K/^{39}K$ mass fractionation corrected measurements of 150 ng samples of K on a customized TIMS platform. The method scales well to lower sample sizes, but likely encounters a significant reproducibility barrier from abundance sensitivity related issues for bigger samples. A comparison of the reproducibility of the method with the expected levels of anomalies related to the *in situ* decay of ^{41}Ca and ^{40}K spallogenic overprint indicates that the method has the nescessary reproducibility to resolve and quantify these types of anomalies in refractory inclusions.

Although the additional dynamic range coupled with increased sensitivity afforded by a mix of 10^{10} Ω, 10^{11} Ω and 10^{12} Ω resistors should theoretically lead to measurements conducted comfortably in the poisson-noise dominated regime, deconvolution of the fundamental JN- and poisson-noise components leaves a residual noise component, similar in intensity to the JN-noise on the 10^{12} Ω resistor itself. The exact cause of this shortfall is uncertain, but is most likely due to imperfections in the electronic circuitry itself. As a results, 10^{12} Ω resistors generally only perform as good as $\sim 10^{11.7}$ Ω, with respect to resistor noise, partially negating the advantage of utilizing them.

For high K/Ti samples, a straightforward single step separation of K in 0.5 M hydrochloric media is sufficient for achieving samples of sufficient purity to reach the sensitivity resulting in precise and accurate mass fractionation corrected $^{41}K/^{39}K$ and $^{40}K/^{41}K$ value. For low level K samples with high Ti-content, such as differentiated basaltic meteorites, or the refractory inclusions which are the main target of analysis, Ti-separation is necessary to achieve full sensitivity and the added precision and accuracy that follows.

5 Acknowledgments

Financial support for this project was provided by the Danish National Research Foundation, the Danish Natural Science

Published on 11 November 2010 on http://pubs.rsc.org | doi:10.1039/C0JA00067A
Downloaded by New Copenhagen University on 26 February 2011

 This journal is © The Royal Society of Chemistry 2011

View Online

Research Council, and the University of Copenhagen's Programme of Excellence. The Centre for Star and Planet Formation is funded by the Danish National Research Foundation and the University of Copenhagen's Programme of Excellence. The quality of this article was significantly improved by the comments of J. Fietzke and an anonymous reviewer.

6 References

1 G. Srinivasan, S. Sahijpal, A. A. Ulyanov and J. N. Goswami, *Geochim. Cosmochim. Acta*, 1996, **60**, 1823–1835.
2 S. Sahijpal, J. N. Goswami, A. M. Davis, L. Grossman and R. S. Lewis, *Nature*, 1998, **391**, 559–561.
3 S. Sahijpal, J. N. Goswami and A. M. Davis, *Geochim. Cosmochim. Acta*, 2000, **64**, 1989–2005.
4 G. J. Wasserburg, M. Busso, R. Gallino and K. M. Nollett, *Nucl. Phys. A*, 2006, **777**, 5–69.
5 L. W. Looney, J. J. Tobin and B. D. Fields, *Astrophys. J.*, 2006, **652**, 1755–1762.
6 M. Gounelle, F. H. Shu, H. Shieng, A. E. Glassgold, K. E. Rehm and T. Lee, *Astrophys. J.*, 2001, **548**, 1051–1070.
7 D. D. Clayton and E. Dwek, *Astrophys. J.*, 1977, **214**, 300–315.
8 G. F. Herzog, *Treatise on Geochemistry*, 2003, **1.13**, 347–380.
9 F. W. E. Strelow, J. H. J. Coetzee and C. R. Van Zyl, *Anal. Chem.*, 1968, **40**, 196–199.
10 F. W. E. Strelow, C. J. Liebenberg and A. H. Victor, *Anal. Chem.*, 1974, **46**, 1409–1414.
11 J. Beukenkamp and W. Rieman, *Anal. Chem.*, 1950, **22**, 582–585.
12 B. S. Mohite, D. N. Zambare and B. E. Mahadik, *Anal. Chem.*, 1994, **66**, 4097–4099.
13 F. W. E. Strelow, *Anal. Chem.*, 1960, **32**, 1185–1188.
14 P. J. Sylvester, S. B. Simon and L. Grossman, *Geochim. Cosmochim. Acta*, 1993, **57**, 3763–3784.
15 J. R. de Laeter, J. K. Böhlke, P. De Bivre, H. Hidaka, H. S. Peiser, K. J. R. Rosman and P. D. P. Taylor, *Pure Appl. Chem.*, 2003, **75**, 683–800.
16 E. Anders and N. Grevasse, *Geochim. Cosmochim. Acta*, 1989, **53**, 197–214.
17 K. D. McKeegan and A. M. Davis, *Treatise on Geochemistry*, 2003, **1.16**, 431–460.
18 M. E. Wieser and J. B. Schwieters, *Int. J. Mass Spectrom.*, 2005, **242**, 97–115.
19 J. L. Birck, *Geostand. Geoanal. Res.*, 2001, **25**, 253–259.
20 F. Wombacher and M. Rehkämper, *J. Anal. At. Spectrom.*, 2003, **18**, 1371–1375.
21 E. D. Young, A. Galy and H. Nagahara, *Geochim. Cosmochim. Acta*, 2002, **66**, 1095–1104.
22 A. Trinquier, J.-L. Birck and C. Allegre, *J. Anal. At. Spectrom.*, 2008, **23**, 1565–1574.

Published on 11 November 2010 on http://pubs.rsc.org | doi:10.1039/C0JA00067A
Downloaded by New Copenhagen University on 26 February 2011